Contact resistance and overlapping capacitance in flexible sub-micron long oxide thin-film transistors for above 100 MHz operation

Article (Published Version)

Contact resistance and overlapping capacitance in flexible sub-micron long oxide thin-film transistors for above 100MHz operation

Niko Münzenrieder, Giovanni A. Salvatore, Luisa Petti, Christoph Zysset, Lars Büthe, Christian Vogt, Giuseppe Cantarella, and Gerhard Tröster

Citation: Applied Physics Letters **105**, 263504 (2014); doi: 10.1063/1.4905015
View online: http://dx.doi.org/10.1063/1.4905015
View Table of Contents: http://scitation.aip.org/content/aip/journal/apl/105/26?ver=pdfcov
Published by the AIP Publishing

APPLIED PHYSICS LETTERS **105**, 263504 (2014)

Contact resistance and overlapping capacitance in flexible sub-micron long oxide thin-film transistors for above 100 MHz operation

Niko Münzenrieder,[a),b)] Giovanni A. Salvatore,[b)] Luisa Petti, Christoph Zysset, Lars Büthe, Christian Vogt, Giuseppe Cantarella, and Gerhard Tröster
Electronics Laboratory Swiss Federal Institute of Technology (ETH) Zürich, Gloriastrasse 35, 8092 Zürich, Switzerland

(Received 27 October 2014; accepted 7 December 2014; published online 31 December 2014)

In recent years new forms of electronic devices such as electronic papers, flexible displays, epidermal sensors, and smart textiles have become reality. Thin-film transistors (TFTs) are the basic blocks of the circuits used in such devices and need to operate above 100 MHz to efficiently treat signals in RF systems and address pixels in high resolution displays. Beyond the choice of the semiconductor, i.e., silicon, graphene, organics, or amorphous oxides, the junctionless nature of TFTs and its geometry imply some limitations which become evident and important in devices with scaled channel length. Furthermore, the mechanical instability of flexible substrates limits the feature size of flexible TFTs. Contact resistance and overlapping capacitance are two parasitic effects which limit the transit frequency of transistors. They are often considered independent, while a deeper analysis of TFTs geometry imposes to handle them together; in fact, they both depend on the overlapping length (L_{OV}) between source/drain and the gate contacts. Here, we conduct a quantitative analysis based on a large number of flexible ultra-scaled IGZO TFTs. Devices with three different values of overlap length and channel length down to 0.5 μm are fabricated to experimentally investigate the scaling behavior of the transit frequency. Contact resistance and overlapping capacitance depend in opposite ways on L_{OV}. These findings establish routes for the optimization of the dimension of source/drain contact pads and suggest design guidelines to achieve megahertz operation in flexible IGZO TFTs and circuits. © *2014 AIP Publishing LLC.*
[http://dx.doi.org/10.1063/1.4905015]

The advancements, which have been achieved in materials processing and assembling, have enabled new forms of electronics like flexible displays,[1] electronic papers,[2] smart textiles,[3] stretchable and epidermal sensors,[4] and dissolvable circuits.[5] Different forms of silicon,[6,7] carbon based materials like nanotubes or organic polymers and small molecules,[8–10] or amorphous semiconductors can be used to build such devices.[11,12] Deformable wireless sensors or bendable radio frequency transceivers require electronic circuits which operate in the megahertz regime in order to treat signals, and transmit data. The basic components of all these flexible circuits are thin-film transistors (TFTs) who should be optimized to achieve sufficient electrical and mechanical performance using cost effective fabrication methods. Among the parameters describing the electrical operation of TFTs, the transit frequency, f_T, is one of the most important since it quantifies the speed of the devices. In first approximation, it reads as follows:[13]

$$f_T = \frac{g_m}{2 \times \pi \times C_G} \approx \frac{\mu \times (V_{GS} - V_{TH})}{2 \times \pi \times L_{CH}^2}, \qquad (1)$$

here g_m is the transconductance, μ is the carrier mobility, L_{CH} is the channel length, and $V_{GS} - V_{TH}$ is the gate overdrive voltage of the TFT. The gate capacitance $C_G = C_{GS} + C_{GD}$ is the sum of the gate-to-source and the gate-to-drain capacitance.

For $V_{GS} - V_{TH} = 3$ V and $L_{CH} = 1\ \mu$m, devices based on organic semiconductors have demonstrated a f_T of about 10 MHz since the mobility is in order of 1 $cm^2 V^{-1} s^{-1}$;[10] inorganic semiconductors can reach the gigahertz regime if based on high quality crystalline semiconductors,[6,14] but such merits usually come at the expense of complex fabrication methods;[6,9,10,15] graphene and transition metal dichalcogenides promise high mobility[16] but the technology development is still at its infancy.[17] TFTs based on amorphous oxide semiconductors like Indium-Gallium-Zinc-Oxide (IGZO) are an alternative since they can be manufactured on large-scale substrates and provide mobilities >10 $cm^2 V^{-1} s^{-1}$ which, according to Eq. (1) leads to a f_T of ≈500 MHz (assuming a channel length of 1 μm, an over-bias voltage of 2 V, and a carrier mobility of 15 $cm^2 V^{-1} s^{-1}$).[12] Beyond the choice of the semiconductor, the design and geometry especially of flexible junctionless thin-film transistors impose some limitations. The parameters of Eq. (1) are affected by the contact resistance R_C, and parasitic overlap capacities C_{OV}, between the gate and source/drain metallization (Fig. 1). In flexible devices, these overlaps are caused by the fabrication on mechanically and thermally instable flexible substrates.[18] This leads to the fact that f_T values for 1 μm-long IGZO TFTs are <100 MHz (Figure S2(d)[19]).[20,21] In fact, if the channel length is reduced below 1 μm the channel resistance becomes smaller than the contact resistance, thus causing the effective mobility μ_{eff}, to drop. This can be modelled as follows:[22]

[a)]Email: muenzenrieder@ife.ee.ethz.ch
[b)]N. Münzenrieder and G. A. Salvatore contributed equally to the work.

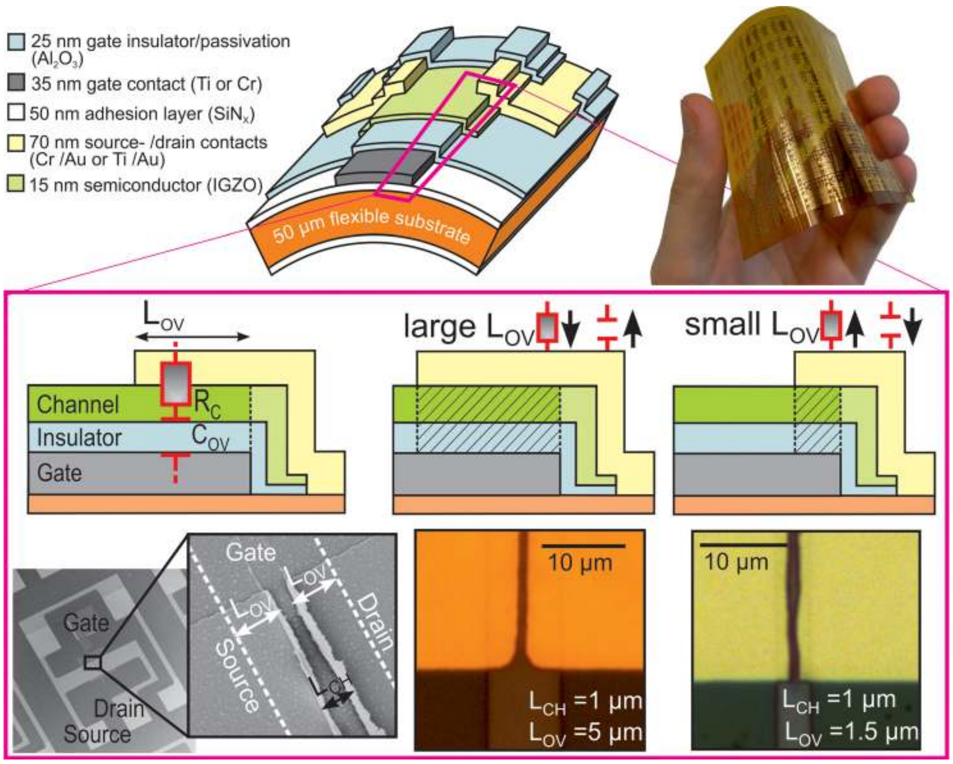

FIG. 1. Flexible bottom-gate TFT fabricated on free-standing plastic foil. The channel length L_{CH}, and width W set the channel resistances and capacitance (R_C and C_{CH}). The overlap length L_{OV} defines the source/drain to gate overlap, and determines the contact resistances R_{CH}, and overlap capacitance C_{OV}. The SEM image shows a flexible IGZO TFT whose channel length is only 0.5 μm. The optical microscope images show two devices with two different L_{OV}.

$$\mu_{eff} = \frac{\mu}{1 + \mu \times C_{OX} \times \frac{W}{L_{CH}} \times (V_{GS} - V_{TH}) \times \Re_{C\{L_{OV}\}}}, \quad (2)$$

whereas $\Re_{C\{L_{OV}\}}$ is a function of the overlapping length between gate and source/drain (L_{OV}), describing the contact resistance. Similarly, the channel capacitance decreases while the parasitic overlap capacitance remains constant if the channel length is reduced. Although the influence of device scaling on C_{OV} and R_C is widely described in literature, the two parameters are usually treated separately. However, a deeper analysis of the TFT geometry reveals that, due to the carrier accumulation layer between gate and source/drain contacts in staggered TFTs, C_{OV} and R_C are not independent from each other and they both directly depend on L_{OV}.[10,23]

Here, we conduct a quantitative analysis based on a large number of flexible ultra-scaled IGZO TFTs. Flexible devices with three different values of overlap length and channel length down to 0.5 μm are fabricated to investigate the scaling behavior of the transit frequency. A model is developed to predict the effects of scaling and to identify resistance- and capacitance-dominated regions. Systematic evaluation of the experimental data and accurate modeling reveal that R_C and C_{OV} are not independent and they depend on L_{OV} in opposite ways. This study establishes routes for the optimization of the dimension of source/drain contact pads of junctionless transistors and demonstrates design guidelines to achieve operation of TFTs and circuits in the megahertz regime.

The flexible transistors investigated in this study are presented in Fig. 1. TFTs are fabricated on free-standing polyimide foil using metallic contacts, Al_2O_3 as gate insulator and passivation, and IGZO as semiconductor. Layer structuring was done by conventional and self-aligned lithography. The fabrication process is described elsewhere.[18,21] The TFTs exhibit channel length between 10 μm and 0.5 μm, and gate to source/drain overlaps L_{OV} of 15 μm, 5 μm, and 1.5 μm. These dimensions are limited by the deformation of the flexible substrate during the fabrication process. Here, L_{CH} is defined as the distance between the metallic source/drain contacts and was measured using an optical microscope and an SEM. The DC performance of the resulting TFTs is shown in supplementary Fig. S1.[19] The transistors exhibit an average effective mobility μ_{eff} of $\approx$15 $cm^2 V^{-1} s^{-1}$ and a threshold voltage V_{TH} around 0.45 V (extracted using the Shichman–Hodges model of the TFT current[13]). The transistors continue to work when bent to a tensile radius of 3.5 mm which corresponds to 0.5% strain (supplementary Fig. S3[19]).[7,12,21,24] Larger strain causes cracks and destroys the TFTs permanently.[18] Due to the ratio between the lateral structure sizes and the layer thicknesses of the TFTs (Fig. 1), as well as because of the obtained TFT characteristics, short channel effects are assumed to be negligible.

Since analog circuits, in particular, amplifiers, have to deliver a high gain and operation frequency, TFTs with high f_T, g_m, and internal gain g_m/g_{ds} (with output resistance g_{ds}) are desired. The important dimensional parameters, influencing the electrical performance, are the gate to source/drain overlap length L_{OV}, and the channel length L_{CH} and width W. Shorter TFT channels increase g_m, and decrease the channel capacitance simultaneously, leading to improved transit frequencies. W influences the absolute drain current, but not the AC performance. L_{OV} determines the contact area between the source/drain metallization and the size of the accumulation layer inside the IGZO. This area influences the parasitic gate to source/drain overlap capacities C_{OV} and the contact resistance R_C. Additionally, the contact resistance can, for example, also be influenced by the

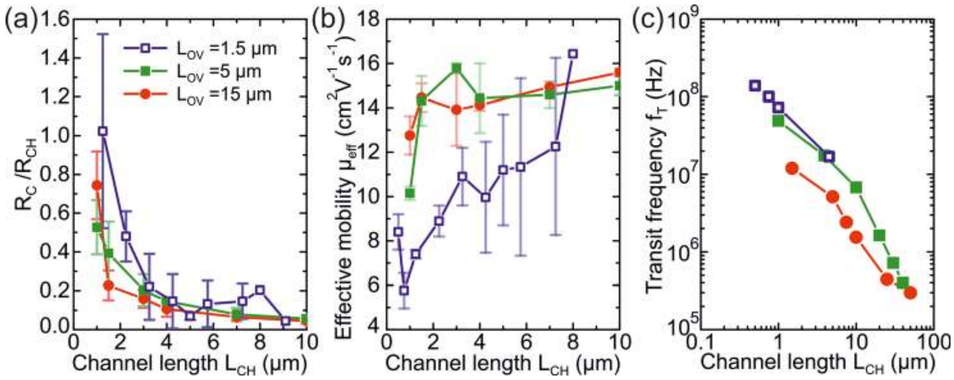

FIG. 2. Performance of IGZO TFTs. (a) Ratio between contact- and channel resistance R_C/R_{CH} as function of L_{CH} for TFTs with different L_{OV}. For small channel length the R_C/R_{CH} ratio becomes larger than 1 and results in a drop of the effective mobility (b). (c) Transit frequency f_T of flexible TFTs with different channel dimensions. f_T was extracted from the current-gain h_{21} (calculated from measured S-parameters). The transit frequency was extracted as the unity-gain frequency of the current-gain h_{21} (Fig. S2(d)[19]).

electronic properties of the contact metal,[25] or by plasma and heat treatments.[26] The presented TFTs with optimized Ti/Au and Cr/Au contacts exhibit state-of-the-art width-normalized contact resistances of 5.6 Ω cm ($L_{OV} = 15\,\mu$m), 6.7 Ω cm ($L_{OV} = 5\,\mu$m), and 12.4 Ω cm ($L_{OV} = 1.5\,\mu$m).[22,27] R_C was extracted using the transmission-line method.[28] As shown in Fig. 2(a), R_C can reach values comparable to the channel resistance of short channel TFTs ($L_{CH} \lesssim 2\,\mu$m), and reduce μ_{eff} to values $<10\,\mathrm{cm^2\,V^{-1}\,s^{-1}}$ (Fig. 2(b)).[22,29] Contrary to this Fig. 2(c) shows an increase of f_T with decreasing L_{OV}. This reflects the influence of the gate capacitance on f_T (Eq. (1)). Since C_{OV} directly contributes to the gate capacitance and is proportional to L_{OV}, small L_{OV} values are beneficial. Overall, it can be concluded that the opposing effects of L_{OV} on the capacitance and the resistance, require efforts to optimize the TFT AC performance.

A similar trade-off is necessary when TFTs are used as building blocks for flexible circuits. The influence of the TFT dimensions on the width-normalized transconductance and the internal gain is shown in Figs. 3(a) and 3(b). High contact resistances caused by small overlap length reduce g_m and increase g_{ds}. To demonstrate the consequences of TFT scaling on the performance of circuits flexible common source amplifiers, shown in Fig. 3(c), have been fabricated. Fig. 3(d) shows Bode plots of circuits based on flexible IGZO TFTs with the following dimensions: Circuit 1: $L_{CH} = 2.5\,\mu$m, $L_{OV} = 5\,\mu$m; circuit 2: $L_{CH} = 2.5\,\mu$m, $L_{OV} = 1.5\,\mu$m; and circuit 3: $L_{CH} = 0.5\,\mu$m, $L_{OV} = 1.5\,\mu$m. All amplifiers were tested by applying a sinusoidal input signal with a peak-to-peak amplitude of 100 mV and a supply voltage of 5 V. The output was monitored with an oscilloscope, using an output load of 2 pF and 1 MΩ. The TFTs of circuit 1 exhibit a transit frequency of ≈20 MHz, and an internal gain around 50, the circuit has a voltage gain A_V of 7 dB, and a unity gain frequency f_0 of 1.5 MHz resulting in a gain-bandwidth product GBWP of 3.4 MHz. The reduction of the overlap in circuit 2 ($f_T \approx 35$ MHz, $g_m/g_{ds} \approx 10$) leads to a higher f_0 (3.2 MHz) but slightly smaller A_V (3.1 dB) resulting in an improved GBWP of 6.4 MHz. Further scaling of the TFTs in circuit 3 ($f_T \approx 130$ MHz, $g_m/g_{ds} \approx 2$) again increases f_0 (4 MHz) but also reduces A_V to 2.7 dB and the GBWP to 5.4 MHz. This demonstrates that smaller TFT dimensions are not necessarily beneficial for the performance of the circuits.

The optimization of the TFT AC performance requires device dimensions with an ideal combination of L_{CH} and L_{OV}, to ensure an optimal tradeoff between C_G and R_C. Therefore, the effects of the device geometry on C_G and R_C have to be included into Eqs. (1) and (2). Similar to a plate capacitor, the width-normalized gate capacitance and the channel dimensions are linked by the following formula:[13]

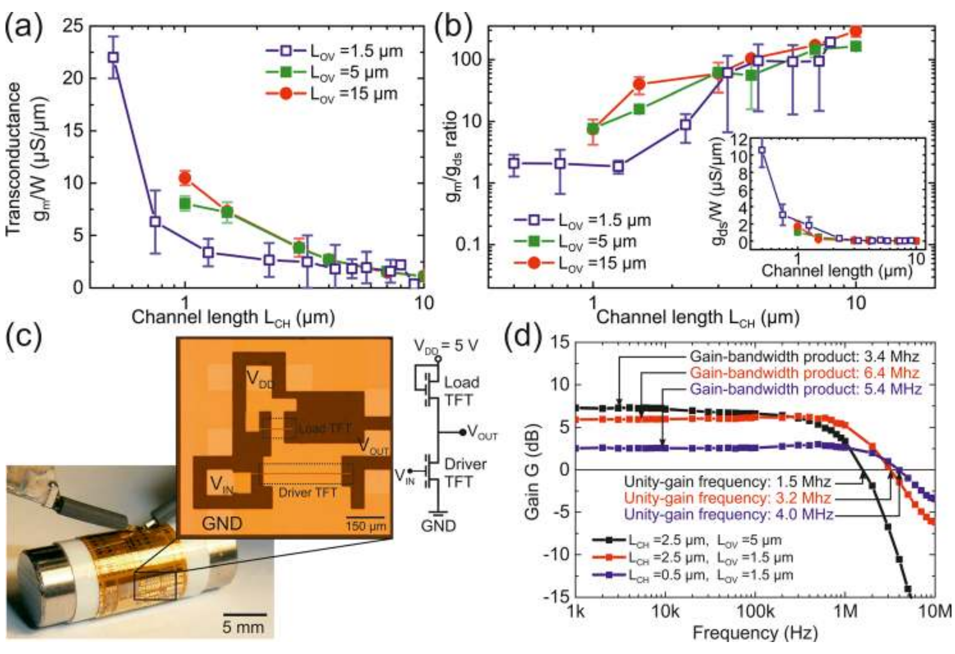

FIG. 3. (a) Width-normalized transconductance g_m/W for different L_{OV} and L_{CH}. (b) The internal gain g_m/g_{ds} (output resistance g_{ds} shown in inset) decreases for small L_{OV} and small L_{CH}. (c) Schematic and micrograph of a flexible common source amplifier. (d) Bode plots of common source amplifiers with different channel dimensions.

$$C_G = C_{OX} \times (2 \times L_{OV} + L_{CH}). \quad (3)$$

Additionally, based on the present measurements, the correlation between L_{OV} and R_C is modeled by an exponential function:[30]

$$\Re_{C\{L_{OV}\}} = A + B \times e^{-C \times L_{OV}}, \quad (4)$$

with A, B, and C as fitting constants. The contact resistances of the presented TFTs result in the following fitted values (supplementary Fig. S2(c)[19]): $A = 5.6\ \Omega$ cm, $B = 12.6\ \Omega$ cm, and $C = 0.414\ \mu m^{-1}$.

Accordingly, the following expression for f_T of flexible IGZO TFTs can be derived:

$$f_T = \left[\frac{g_{m,0}}{2 \times \pi \times C_{OX} \times L_{CH}^2}\right] \times \left[\frac{L_{CH}}{L_{CH} + 2 \times L_{OV}}\right] \times \left[\frac{L_{CH}}{L_{CH} + g_{m,0} \times \Re_{C\{L_{OV}\}}}\right] \equiv f_{T,0} \times \mathbb{f}_C \times \mathbb{f}_R \quad (5)$$

Here, C_{OX} is the oxide capacitance and $g_{m,0} = \mu_0 \times C_{OX} \times (V_{GS} - V_{TH})$ the width-normalized intrinsic transconductance at a given bias point. Equation (5) is split into three independent factors which are defined as follows: $f_{T,0}$ is the transit frequency of an ideal TFT (with $R_C = 0\ \Omega$ cm, and $C_{OV} = 0$ F μm^{-1}), whereas $\mathbb{f}_C$ and $\mathbb{f}_R$ are factors <1 describing the destructive influence of C_{OV} and R_C.

Equation (5) can predict the effects of scaling flexible IGZO TFTs with unchanged layer structure. Fig. 4(a) displays the modeled f_T for different combinations of L_{CH} and L_{OV}. Besides the absolute f_T calculation, the developed model also determines the influence of R_C and C_{OV}. Fig. 4(b) visualizes the factors $f_{T,0}$, $\mathbb{f}_C$, and $\mathbb{f}_R$, and validates Eq. (5) by showing good agreement between calculated and measured transit frequency. Additionally, it illustrates that R_C is dominating the TFT AC performance for $L_{CH} \lesssim 1\ \mu m$, which leads to a saturation of f_T. The relative influence of R_C and C_{OV} on f_T depends on L_{CH} and L_{OV}, and is quantified by the ratio between $\mathbb{f}_C$ and $\mathbb{f}_R$. This ratio is plotted in Fig. 4(c). TFTs with $L_{OV} > 1\ \mu m$ are dominated by the parasitic overlap capacities ($\mathbb{f}_C/\mathbb{f}_R < 1$), whereas TFTs with $L_{OV} < 1\ \mu m$ are mainly influenced by the contact resistance ($\mathbb{f}_C/\mathbb{f}_R > 1$). The transition between resistance and capacitance dominated AC performance at $L_{OV} = 1\ \mu m$ is independent from the TFT channel length. Hence, the fabrication of IGZO TFTs with gate to source/drain overlaps $<1\ \mu m$ is only effective if the specific contact resistance can be decreased.

In conclusion, we studied the contact resistance and overlapping capacitance in flexible TFTs and their effect on the transit frequency. Transistors and circuits with three different values of overlap length, and channel length down to $0.5\ \mu m$ were fabricated on free-standing plastic foil. Experimental data and modeling confirms that R_C and C_{OV} both directly depend on the overlapping length and that they cannot be optimized independently in junctionless thin-film transistors. Based on these findings, the limits of effective scaling of current flexible IGZO TFTs were explored and design guidelines to achieve an optimal trade-off between C_G and R_C for high speed device and circuit operation were suggested.

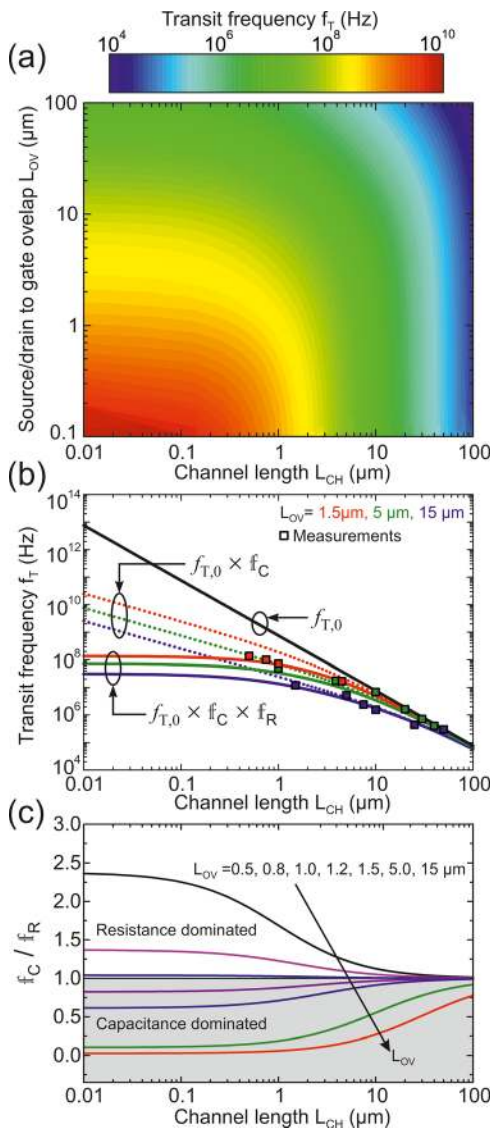

FIG. 4. Design guidelines to achieve transit frequency higher than 100 MHz in IGZO TFTs. (a) Calculated transit frequency of TFTs with different channel dimensions. The model considers the influence of the parasitic overlap capacities and the contact resistance. (b) Modeled influence of the overlap capacitance ($\mathbb{f}_C$) and the contact resistance ($\mathbb{f}_R$) on the transit frequency according to Eq. (5), and comparison with measured f_T values. (c) $\mathbb{f}_C/\mathbb{f}_R$ for different L_{CH} and L_{OV} values. The ratio between $\mathbb{f}_C$ and $\mathbb{f}_R$ shows the dominating influence of the contact resistance ($\mathbb{f}_C/\mathbb{f}_R > 1$) in TFT with $L_{OV} < 1\ \mu m$.

This work was supported by the European Commission through the FP7 Project "flexible multifunctional bendable integrated light-weight ultrathin systems" under Contract FP7-287568.

[1]S. Bae, H. Kim, Y. Lee, X. Xu, J.-S. Park, Y. Zheng, J. Balakrishnan, T. Lei, H. Ri Kim, and Y. Il Song, Nat. Nanotechnol. **5**(8), 574 (2010); G. H. Gelinck, H. E. A. Huitema, E. Van Veenendaal, E. Cantatore, L. Schrijnemakers, J. B. P. H. Van der Putten, T. C. T. Geuns, M. Beenhakkers, J. B. Giesbers, B. H. Huisman, E. J. Meijer, E. M. Benito, F. J. Touwslager, A. W. Marsman, B. J. E. Van Rens, and D. M. De Leeuw, Nat. Mater. **3**(2), 106 (2004).

[2]J. A. Rogers, Z. Bao, K. Baldwin, A. Dodabalapur, B. Crone, V. R. Raju, V. Kuck, H. Katz, K. Amundson, J. Ewing, and P. Drzaic, Proc. Natl. Acad. Sci. U.S.A. **98**(9), 4835 (2001).

[3]K. Cherenack, C. Zysset, T. Kinkeldei, N. Münzenrieder, and G. Tröster, Adv. Mater. **22**(45), 5178 (2010).

[4]C. Wang, D. Hwang, Z. Yu, K. Takei, J. Park, T. Chen, B. Ma, and A. Javey, Nat. Mater. **12**(10), 899 (2013); D.-H. Kim, N. Lu, R. Ma, Y.-S. Kim, R.-H. Kim, S. Wang, J. Wu, S. M. Won, H. Tao, A. Islam, K. J. Yu, T. Kim, R. Chowdhury, M. Ying, L. Xu, M. Li, H.-J. Chung, H. Keum, M. McCormick, P. Liu, Y.-W. Zhang, F. G. Omenetto, Y. Huang, T. Coleman, and J. A. Rogers, Science **333**(6044), 838–843 (2011).

[5]S. W. Hwang, H. Tao, D. H. Kim, H. Y. Cheng, J. K. Song, E. Rill, M. A. Brenckle, B. Panilaitis, S. M. Won, Y. S. Kim, Y. M. Song, K. J. Yu, A. Ameen, R. Li, Y. W. Su, M. M. Yang, D. L. Kaplan, M. R. Zakin, M. J. Slepian, Y. G. Huang, F. G. Omenetto, and J. A. Rogers, Science **337**(6102), 1640 (2012).

[6]D. H. Kim, J. H. Ahn, W. M. Choi, H. S. Kim, T. H. Kim, J. Z. Song, Y. G. Y. Huang, Z. J. Liu, C. Lu, and J. A. Rogers, Science **320**(5875), 507 (2008).

[7]H. Gleskova, S. Wagner, and Z. Suo, J. Non-Cryst. Solids **266**, 1320 (2000).

[8]C. Wang, J. C. Chien, K. Takei, T. Takahashi, J. Nah, A. M. Niknejad, and A. Javey, Nano Lett. **12**(3), 1527 (2012); M. Kaltenbrunner, T. Sekitani, J. Reeder, T. Yokota, K. Kuribara, T. Tokuhara, M. Drack, R. Schwodiauer, I. Graz, S. Bauer-Gogonea, S. Bauer, and T. Someya, Nature **499**(7459), 458 (2013).

[9]T. Sekitani, U. Zschieschang, H. Klauk, and T. Someya, Nat. Mater. **9**(12), 1015 (2010).

[10]F. Ante, D. Kalblein, T. Zaki, U. Zschieschang, K. Takimiya, M. Ikeda, T. Sekitani, T. Someya, J. N. Burghartz, K. Kern, and H. Klauk, Small **8**(1), 73 (2012).

[11]G. A. Salvatore, N. Münzenrieder, T. Kinkeldei, L. Petti, C. Zysset, I. Strebel, L. Büthe, and G. Tröster, Nat. Commun. **5**, 2982 (2014); E. Fortunato, P. Barquinha, and R. Martins, Adv. Mater. **24**(22), 2945 (2012).

[12]K. Nomura, H. Ohta, A. Takagi, T. Kamiya, M. Hirano, and H. Hosono, Nature **432**(7016), 488 (2004).

[13]S. M. Sze and K. K. Ng, *Physics of Semiconductor Devices*, 3rd ed. (Wiley-Interscience, Hoboken, N.J., 2007), pp. 303; 348.

[14]C. Wang, K. Takei, T. Takahashi, and A. Javey, Chem. Soc. Rev. **42**(7), 2592 (2013); A. E. Khorasani, T. L. Alford, and D. K. Schroder, IEEE Trans. Electron Devices **60**(8), 2592 (2013).

[15]E. A. Angelopoulos, M. Zimmermann, W. Appel, S. Endler, S. Ferwana, C. Harendt, T. Hoang, A. Pruemm, and J. N. Burghartz, Int. Electron Devices Meet. **2010**, 2.5.1.

[16]C. R. Dean, A. F. Young, I. Meric, C. Lee, L. Wang, S. Sorgenfrei, K. Watanabe, T. Taniguchi, P. Kim, and K. L. Shepard, Nat. Nanotechnol. **5**(10), 722 (2010); K. S. Novoselov, A. K. Geim, S. V. Morozov, D. Jiang, Y. Zhang, S. V. Dubonos, I. V. Grigorieva, and A. A. Firsov, Science **306**(5696), 666 (2004); H.-Y. Chang, S. Yang, J. Lee, L. Tao, W.-S. Hwang, D. Jena, N. Lu, and D. Akinwande, ACS Nano **7**, 5446 (2013); G. A. Salvatore, N. Münzenrieder, C. Barraud, L. Petti, C. Zysset, L. Büthe, K. Ensslin, and G. Troester, ACS Nano **7**, 8809 (2013); H. Fang, S. Chuang, T. C. Chang, K. Takei, T. Takahashi, and A. Javey, Nano Lett. **12**(7), 3788 (2012).

[17]Y. Wu, K. A. Jenkins, A. Valdes-Garcia, D. B. Farmer, Y. Zhu, A. A. Bol, C. Dimitrakopoulos, W. Zhu, F. Xia, P. Avouris, and Y. M. Lin, Nano Lett. **12**(6), 3062 (2012); Q. H. Wang, K. Kalantar-Zadeh, A. Kis, J. N. Coleman, and M. S. Strano, Nat. Nanotechnol. **7**(11), 699 (2012).

[18]N. Münzenrieder, L. Petti, C. Zysset, T. Kinkeldei, G. A. Salvatore, and G. Tröster, IEEE Trans. Electron Devices **60**(9), 2815 (2013).

[19]See supplementary material at http://dx.doi.org/10.1063/1.4905015 for more information about the TFT AC and DC characteristics and the influence of mechanical strain.

[20]K. Nomura, T. Kamiya, and H. Hosono, Thin Solid Films **520**(10), 3778 (2012).

[21]N. Münzenrieder, L. Petti, C. Zysset, G. A. Salvatore, T. Kinkeldei, C. Perumal, C. Carta, F. Ellinger, and G. Tröster, IEEE Int. Electron Devices Meet. **2012**, 5.2.1.

[22]E. N. Cho, J. H. Kang, and I. Yun, Curr. Appl. Phys. **11**(4), 1015 (2011).

[23]Y. Xu, C. Liu, W. Scheideler, P. Darmawan, S. L. Li, F. Balestra, G. Ghibaudo, and K. Tsukagoshi, Org. Electron. **14**(7), 1797 (2013).

[24]N. Münzenrieder, K. H. Cherenack, and G. Tröster, IEEE Trans. Electron Devices **58**(7), 2041 (2011).

[25]Y. Shimura, K. Nomura, H. Yanagi, T. Kamiya, M. Hirano, and H. Hosono, Thin Solid Films **516**(17), 5899 (2008).

[26]B. Du Ahn, H. S. Shin, H. J. Kim, J. S. Park, and J. K. Jeong, Appl. Phys. Lett. **93**(20), 203506 (2008).

[27]K. H. Choi and H. K. Kim, Appl. Phys. Lett. **102**(5), 052103 (2013).

[28]W. S. Kim, Y. K. Moon, K. T. Kim, J. H. Lee, B. D. Ahn, and J. W. Park, Thin Solid Films **518**(22), 6357 (2010).

[29]M. Marinkovic, D. Belaineh, V. Wagner, and D. Knipp, Adv. Mater. **24**(29), 4005 (2012).

[30]H. Wang, L. Li, Z. Y. Ji, C. Y. Lu, J. W. Guo, L. Wang, and M. Liu, IEEE Electron Device Lett. **34**(1), 69 (2013).